# Reusable and Closed-Loop Recyclable Underwater Adhesives via Printable Multi-Dynamic Networks Shuxue Wang, a Xiaochun Wu, a Jingjing Li, a Jun Zhao, a Suxu Wang, a Yuke Sun, a Zhihang Wang, \*,b,c & Xiaofeng Xu\*,a <sup>a</sup> College of Materials Science and Engineering, Ocean University of China, Qingdao 266100, China. <sup>b</sup> School of Engineering, College of Science and Engineering, University of Derby, Markeaton Street, Derby DE22 3AW, United Kingdom. <sup>c</sup> Department of Materials Science and Metallurgy, University of Cambridge, Cambridge, CB3 0FS, United Kingdom. \* Corresponding authors: X. Xu, email: xuxiaofeng@ouc.edu.cn Z. Wang, email: z.wang@derby.ac.uk

#### **ABSTRACT**

1

2

3

4

5

6

7

8

9

10

11

12

13

14

15

16

17

Sustainable underwater adhesives have attracted wide attention in fields such as marine exploration and biomedicine. The development of recyclable underwater adhesives that can achieve strong and durable adhesion to various substrates is a daunting challenge. Herein, a series of recyclable underwater adhesives are developed through synergistic engineering of molecular design and multiple dynamic cross-linking networks. The selected well-designed adhesives exhibit excellent underwater adhesion on a variety of substrates, achieving a maximum adhesion strength up to 3.31 MPa. By integrating dynamic covalent and noncovalent cross-links, the adhesive demonstrates rapid self-healing, on-demand reversible adhesion/desorption, and consistent adhesion performance over more than 30 reuse cycles. Moreover, dynamic disulfide bonds impart dual closed-loop recyclability to the adhesive: chemical recycling achieves up to 89.6% monomer recovery, while physical recycling through melt reprocessing allows for effective reuse of adhesive waste. Furthermore, these adhesives exhibit 3D printability, thereby underscoring their great potential for creating customizable underwater adhesives. This study offers new insights into the development of recyclable underwater adhesives that combine strong, repeatable adhesion and desorption with 3D printing capabilities, paving the way for their broader adoption in practical applications.

18

19

20

**Keywords:** tape-type adhesives, underwater adhesion, switchable adhesion, recyclable adhesion, 3D printable adhesives

21

22

23

## 1. Introduction

1

2

3

4

5

6

7

8

9

10

11

12

13

14

15

16

17

18

19

20

21

22

23

24

25

Advanced adhesives are essential technologies across industrial and biomedical fields. While traditional adhesives can form high-strength bonds on dry surfaces, their performance often declines significantly in aqueous environments. This deterioration is primarily caused by interfacial hydration layers that prevent intimate contact, disruption of interfacial interactions by water molecules, and prolonged water infiltration. These physical processes can lead to plasticization, swelling, erosion, or hydrolysis—ultimately resulting in cohesive failure[1-6]. Compared to adhesion in dry conditions, achieving robust bonding on wet surfaces presents far greater challenges. The development of adhesives that maintain strong, durable, and longlasting performance underwater remains a central scientific and engineering problem in the field of adhesive materials[7]. In response to growing demands in sectors such as biomedicine, marine engineering, and energy, underwater adhesives have seen rapid advances in recent years. These new generation of adhesive materials now play critical roles in a range of applications, including aqueous energy devices, antifouling coatings, underwater infrastructure repair, and subsea sensing systems[8-14]. Certain organisms in nature have evolved specialized biological tissues that employ a combination of micro-/nanostructures and physical or chemical interactions to establish stable adhesive interfaces on wet substrates[15-19]. Inspired by the composition and hierarchical architecture of these natural adhesive systems, the design and synthesis of biomimetic underwater adhesives have advanced significantly[20-22]. However, most of the existing underwater adhesives exhibit limited reversibility, with both cycling performance and adhesion strength remaining constrained[23-25]. Fundamentally, this limitation stems primarily from three contributing factors: (i) Physically, the interfacial hydration layer on submerged substrates prevents direct molecular contact between adhesive and surface, promoting adhesive debonding over time. Additionally, this layer exhibits rapid selfreconstruction after disruption, forming a dynamic interfacial barrier that continuously undermines bond integrity during cyclic loading. Together, these physical effects impose inherent limitations on both adhesive efficiency and the recyclability of underwater bonding systems[26]. (ii) Chemically, the irreversible covalent bonds relied on in the commonly used adhesion mechanism only work during the first adhesion and are difficult to support subsequent adhesion cycles[27-29]. Even with the incorporation of dynamic non-covalent interactions to enhance reversibility, the depletion or deactivation of active binding groups after the first use leads to a substantial decline in adhesion strength during reuse[30, 31]. (iii) high-strength underwater adhesives rely covalent As many on strong electrostatic/coordination bonds to achieve robust adhesion, mechanically, their inherent irreversibility under operational conditions often results in cumulative damage through microcrack propagation, polymer chain slippage, or pore formation during cycling[7]. Hence, the abovementioned three failure mechanisms can fundamentally limit the reusability of the adhesives. Overcoming these constraints to develop adhesives that combine both high strength and reversible adhesion would enable transformative advances in subaqueous technologies, enhancing operational versatility, environmental resilience, sustainable resource utilization, and cost-effectiveness across a wide range of subaqueous applications. From a large scaling perspective, the environmental impact and sustainability concerns associated with underwater adhesive systems have also become increasingly prominent[32-35]. The traditional underwater adhesives, including cyanoacrylates, epoxies, and polyurethanes, are difficult to remove from the adhesive substrate at the end of their service life due to their stable cross-linked networks and strong interfacial interactions (e.g., covalent bonds and intermolecular forces). As a result, they eventually become persistent, nondegradable waste, posing serious environmental and resource problems[36-39]. To tackle these challenges, a variety of recyclable adhesives have emerged based on dynamic covalent

1

2

3

4

5

6

7

8

9

10

11

12

13

14

15

16

17

18

19

20

21

22

23

24

networks, encompassing disulfide bonds[40, 41], ester exchange[42, 43], dynamic borate[44], Diels-Alder reaction[45, 46], and Schiff base[47, 48]. With such designs, the dynamic bond exchange between crosslinking points can occur under mild conditions or be selectively dissociated and reconfigured via external stimuli (e.g., heat, light, or specific chemical environments)[49-52]. For instance, upon activation, these mechanisms can induce topological rearrangement and stress relaxation within the network, enabling on-demand interfacial debonding, self-healing of the adhesive interface after damage, and material recycling after disposal. However, despite the abovementioned recent advances, reversible adhesives still face critical limitations in balancing performance with recyclability. Specifically, achieving strong underwater adhesion usually requires the formation of a stable covalent network, while recyclability depends on the dynamic dissociation and reconstruction of bonding motifs - two inherently conflicting requirements that are particularly difficult to reconcile under aqueous conditions[27, 53]. Moreover, dynamic bonds often compromise long-term stability under harsh environments (e.g., high salinity, extreme pH, or biofouling), leading to premature degradation or adhesive failure[54-56]. Consequently, the development of underwater adhesives that simultaneously exhibit durability, reusability, and recyclability remains a formidable challenge. Furthermore, conventional template-assisted manufacturing of tape-type underwater adhesives suffers from limited dimensional precision and structural adaptability, constraining their application to complex geometries or multifunctional scenarios[57, 58]. Extrusion-based 3D printing overcomes these limitations by enabling in situ, spatially precise adhesive deposition with controlled alignment, thereby unlocking unprecedented design freedom and functional integration. While this additive manufacturing approach presents a transformative platform for customized adhesive systems, fundamental challenges in material-process compatibility and interfacial engineering still require further investigation[59, 60].

1

2

3

4

5

6

7

8

9

10

11

12

13

14

15

16

17

18

19

20

21

22

23

24

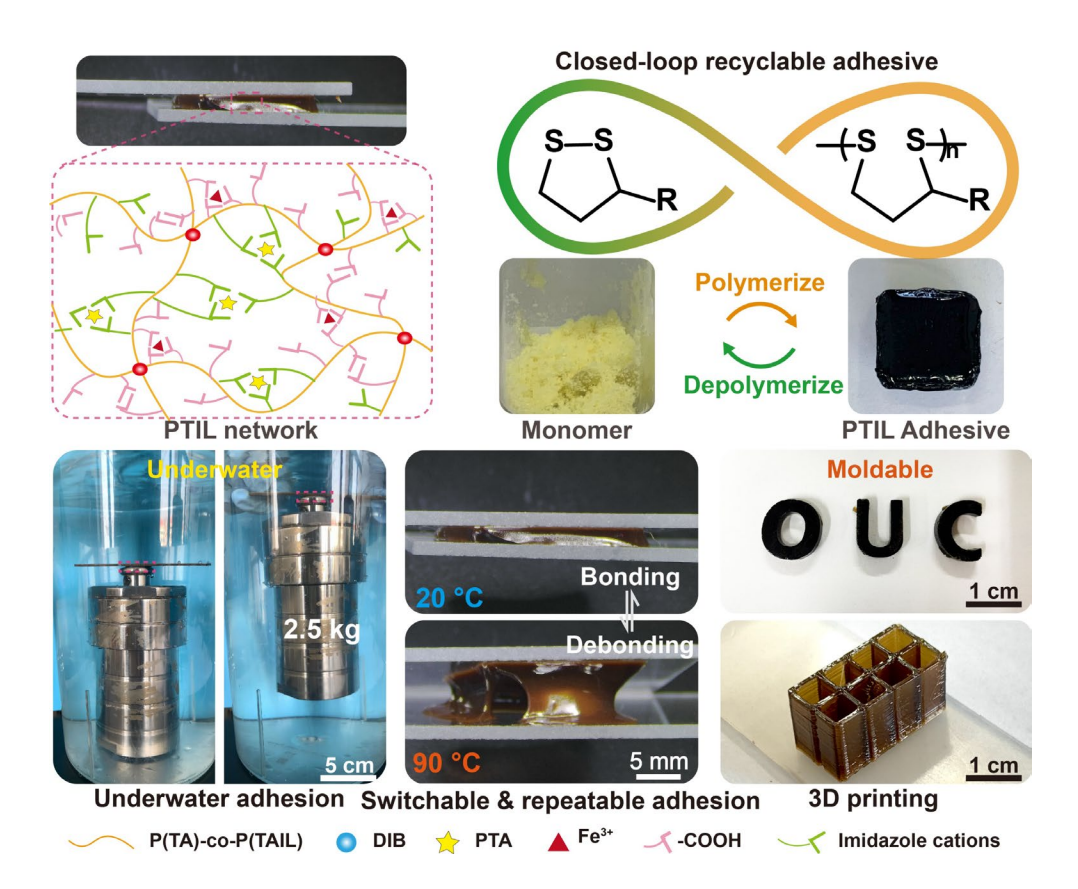


**Fig. 1.** Schematic illustration and digital photographs of reversible polymerization, adhesion strength performance, temperature-deactivated bonding test, and 3D printing of the underwater adhesives developed in this study.

In this study, high-performance underwater adhesives were developed through synergistic molecular design, with further performance optimization via engineering of a multifunctional dynamic crosslinking network. Specifically, the strategic design of thioctic acid (TA) and its ionic liquid derivative (TA-IL) enables solvent-free, thermally activated ring-opening polymerization mediated by dynamic disulfide bonds. At the same time, the incorporation of abundant hydrogen bonding, metal coordination, and electrostatic interactions promotes the formation of physical crosslinks between polymer chains, thereby enhancing the cohesion of the adhesive network. In addition, the inherent dynamism of both the disulfide bonds and the physical crosslinking network endowed switchable adhesion-desorption behavior and intrinsic self-healing properties, thereby enabling on-demand underwater adhesion-desorption and reuse. Moreover, the integration of dynamic disulfide bonds enables two closed-loop recycling

1 pathways that address key sustainability challenges while preserving strong adhesive 2 performance: (i) chemical recycling, which achieves a remarkable monomer recovery rate (up 3 to 89.6%), and (ii) physical recycling, in which melt reprocessing facilitates the efficient reuse 4 of spent material. This synergistic design optimized adhesion, cohesion, and curing kinetics, 5 consequently resulting in rapid-setting, strong (maximum underwater adhesion strength: 3.31 6 MPa), and persistent underwater adhesion on diverse wet substrates. Last but not the least, the 7 dynamic nature of the network provides the capability for constructing programmable 8 structures via 3D printing, highlighting its versatility for customized adhesion applications. 9 Overall, this work underscores the substantial potential of these recyclable adhesives, which 10 combine robust and persistent underwater adhesion with advanced functionalities—including 11 reversible adhesion, self-healing, and 3D printability—thus significantly broadening their 12 applicability in diverse, user-defined scenarios.

# 2. Experimental section

#### 14 **2.1 Material preparation**

13

20

21

22

23

24

25

15 Underwater adhesives (PTIL adhesives): TA (0–0.495 g) and TA-IL (0–0.927 g) were melted 16 at 120 °C. 1,3-diisopropenylbenzene (DIB, 0.1 g) was added and reacted for 5 min at 1500 17 r/min. Then 0.0078 g of FeCl<sub>3</sub> solution was added and reacted for 1 min. Then 0.069 g of 18 phosphotungstic acid (PTA) was added and the reaction continued for 2 min before the mixture 19 was poured into the mold.

#### 2.2 Underwater adhesion characterization

Lap shear adhesion tests: All substrates (glass, plastic and metal) were cleaned with ethanol and deionized water, and then dried using hot-air heating. Glass slides (100 mm × 26 mm × 2 mm) were used as substrates. A glass slide was first immersed in water, followed by application of the adhesive. A second slide was then carefully positioned atop the adhesive without applied pressure, creating a controlled overlap area of either 100 or 225 mm<sup>2</sup>. The

- prepared adhesive joint was then immersed in freshwater or brine for 2 h, without applying
- 2 any additional force. Adhesive joints were characterized using a universal testing system (Al-
- 3 7000MUD) or a force test stand (ESM303, MARK-10) equipped with a digital force gauge
- 4 (M5-100, MARK-10). Force and displacement over time were recorded at a tensile rate of 100
- 5 mm min<sup>-1</sup>. Five samples were measured individually, and the average adhesion strength was
- 6 reported under each condition.

13

21

24

## 2.3 Self-healing characterization

- 8 The adhesive was bisected using a surgical blade, and the two resulting pieces were brought
- 9 into contact in freshwater at 25 °C for a self-healing period of 2 h. The healed specimens were
- subsequently subjected to uniaxial tensile testing, with healing efficiency calculated by
- 11 comparing the recovered mechanical properties to intact samples. A minimum of three
- 12 replicates were tested for each condition.

#### 2.4 Chemical recovery

- 14 Adhesive samples were immersed in a 0.5 M NaOH solution and stirred under ambient
- 15 conditions at room temperature, resulting in a light-brown turbid solution as the dissolution
- progressed. The filtrate containing TA and TA-IL monomers and excess base was treated with
- 17 hydrochloric acid (pH = 3-4) to protonate the TA monomers. The reaction solution was
- allowed to stand to obtain TA and TA-IL monomer precipitates, and then FeCl<sub>3</sub> and PTA were
- washed away repeatedly with pure water. The products were then freeze-dried after filtration
- 20 to finalize TA and TA-IL.

#### 2.5 Heat recovery

- 22 The discarded adhesive was thermally reshaped at 80 °C for 30 min. After cooling to room
- 23 temperature, the form was restored.

#### 2.6 Extrusion-based 3D printing

- 3D structures were modeled by Materialise Magics and sliced by Crua slicing software. The
- 2 molded adhesive was loaded into a stainless-steel syringe (10 mL) and printed using an Allevi
- 3 2 bioprinter through a nozzle (diameter: 0.4 mm) at a print speed of 6 mm s<sup>-1</sup> at a print
- 4 temperature of 95–105 °C. Melt extrusion of the adhesive was controlled by a syringe pump
- 5 with a pressure of 6.0 psi.

7

8 9

10

11

12

13

14

15

16

## 3. Results and discussion

#### 3.1 Fabrication and Characterization of TA-IL Monomers

**Fig. 2.** (a) Synthetic routes of TA-IL monomers and (b) side chain modifications of TA-IL monomers with different ligands.

Thioctic acid (TA) contains a strained five-membered cyclic disulfide moiety capable of undergoing dynamic exchange reactions under external stimuli, thereby conferring unique bond reorganization properties. Upon activation, TA can undergo ring-opening polymerization to form a melt composed of a primary linear dynamic covalent backbone, enabling reversible network formation and material adaptability[61-67]. Moreover, these dynamic disulfide bonds confer plasticity, reversibility, self-healing capability, and stimuli-

responsiveness (heat/light) to materials[68-71], thus provide new opportunities for designing adaptive materials, particularly in applications requiring underwater adhesion. The effectiveness of ionic liquids—particularly those containing fluorine—in underwater adhesion arises from their ability to generate a combination of interfacial interactions, including electrostatic forces, ion-dipole and dipole-dipole interactions, as well as Van der Waals forces. These synergistic interactions collectively enhance both interfacial adhesion and internal cohesive strength[72-77]. Based on its unique structural features, we hypothesized that TA could serve as a modifying agent for ionic liquids, introducing a strained five-membered cyclic disulfide motif. This modification would endow the ionic liquids with stimuli-responsive behavior and the ability to undergo further ring-opening polymerization. Experimentally, capitalizing on the readily modifiable carboxyl groups of TA, a TA-functionalized ionic liquid (TA-IL) featuring an imidazolium moiety and an embedded strained five-membered disulfide ring was synthesized through a straightforward grafting approach. Four ionic liquids with different anionic ligands (Br<sup>-</sup>, TFSI<sup>-</sup>, PF<sub>6</sub><sup>-</sup> and BF<sub>4</sub><sup>-</sup>) containing disulfide five-membered carbocyclic structures were synthesized. The chemical structures and synthetic routes of all compounds are shown in Fig. 2. The chemical structures of all intermediate compounds and monomers were characterized by nuclear magnetic resonance (NMR) (Fig. S1-S7). These results demonstrate that the TA-IL, featuring the disulfide bond five-membered carbon ring structure, were successfully synthesized via imidazolium functionalization of TA and validated our molecular design routine.

1

2

3

4

5

6

7

8

9

10

11

12

13

14

15

16

17

18

19

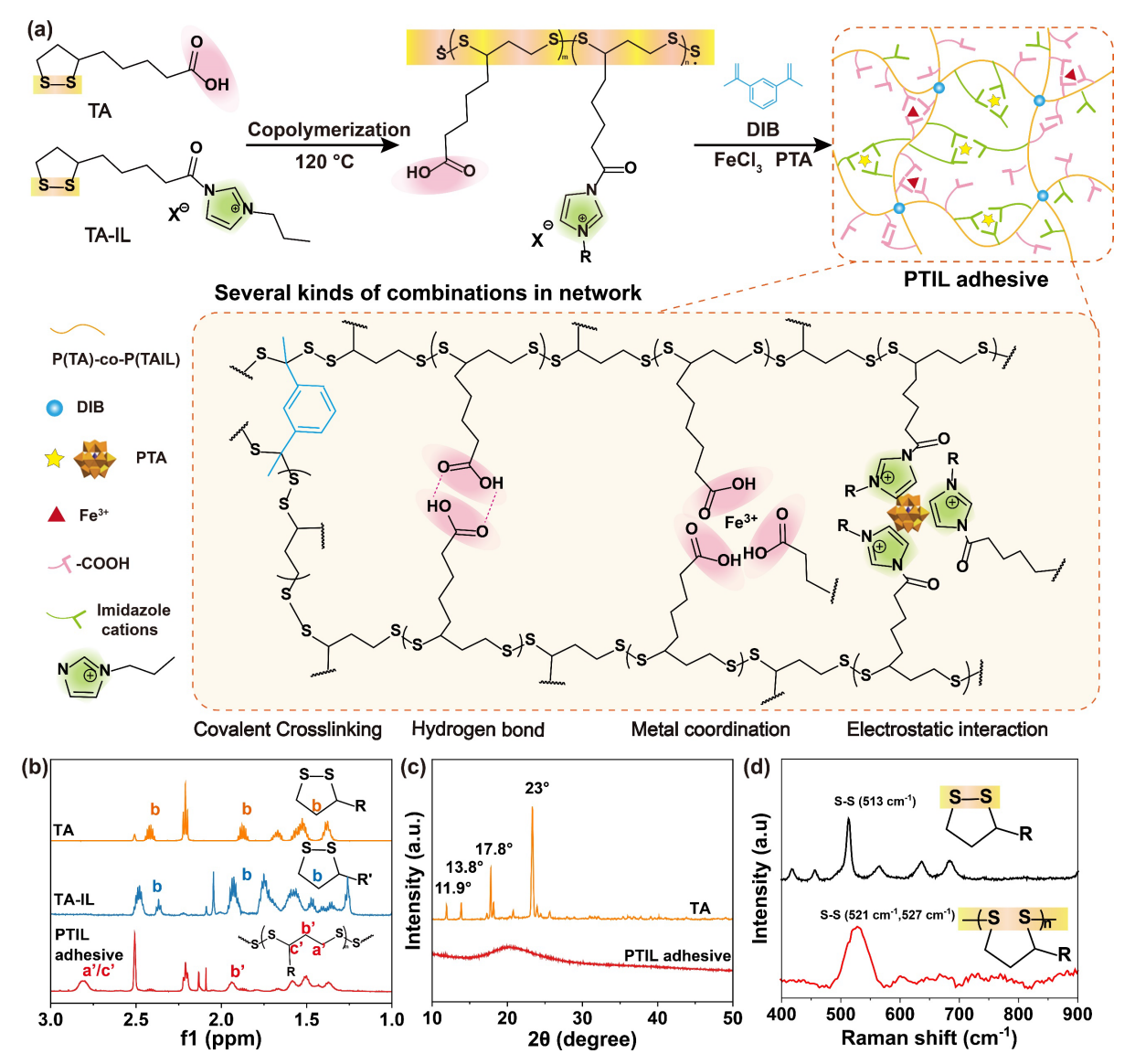


**Fig. 3.** (a) Schematic of preparation and cross-linking reactions for PTIL adhesives; (b) <sup>1</sup>H NMR of TA-IL, TA and PTIL adhesive; (c) XRD of TA and PTIL adhesive; (d) Raman profiles of the monomer and PTIL adhesive.

PTIL were synthesized by a one-pot melting method, in which TA-IL (containing a disulfide five-membered ring) and TA underwent thermally initiated ring-opening polymerization due to dynamic disulfide exchange after complete melting at 120 °C, forming a linear dynamic covalent backbone. Among them, the melting points of TA and TA-IL were tested using differential scanning calorimetry (DSC) to be 63.42 °C and 103 °C, respectively (**Fig. S8** and **S9**), confirming the selected temperature exceeds their melting thresholds. To stabilize the system, divinyl covalent cross-linker DIB was employed to quench terminal diradicals through

reverse vulcanization (Fig. S10), followed by secondary cross-linking mediated by Fe<sup>3+</sup> and 1 2 Phosphotungstic acid (PTA). Here, the hydroxyl termini of TA as dynamic cross-linking sites capable of interacting with hydrogen-bond acceptors or Fe<sup>3+</sup>, demonstrating a great potential 3 for constructing reversibly adaptive polymer networks. The synthesized TA-IL combines the 4 features of a disulfide five-membered carbocyclic ring and an ionic liquid, in which imidazole 5 6 cations can serve as electrostatic cross-linking points to interact with negatively charged cross-7 linking agents. PTA, a structurally clear metal oxide nanocluster, was then incorporated into 8 the adhesives network due to its uniform nanoscale dimensions, high aqueous ionization 9 propensity, and oxo-terminated surfaces conducive to hydrogen-bond formation. Such a 10 molecular structure design fulfills dual functions: (1) providing electrostatic cross-linking sites 11 with imidazolium cations in TA-IL, and (2) contributing abundant hydrogen bonds to enhance 12 the cohesive strength of the PTIL adhesives. 13 The strained disulfide ring in both TA and TA-IL underwent cleavage and subsequent ringopening polymerization, ultimately yielding the PTIL adhesive. This polymerization process 14 was monitored by <sup>1</sup>H NMR spectroscopy (**Fig. 3b**), with characteristic peak shifts confirming 15 16 the disulfide rearrangement and polymer formation. The disulfide five-membered ring of TA 17 and TA-IL opened and underwent ring-opening polymerization to form the final PTIL adhesive. Specifically, methylene (group b, chemical shifts: 2.40 ppm and 1.90 ppm) was 18 19 identified as the characteristic peak of the disulfide five-membered ring structure. Its signal 20 was also used as the NMR probe for open-ring structures toward PTIL formation (group b', 21 chemical shift: 1.93 ppm). The structural evolution of PTIL adhesive was further corroborated 22 by X-ray diffraction (XRD) analysis, which revealed the crystalline-amorphous transition 23 accompanying polymer network formation (Fig. 3c). The TA monomer exhibited a sharp crystalline diffraction peak at ~23°, corresponding to ordered atomic arrangements on crystal 24 25 surfaces. In contrast, the dynamically crosslinked PTIL adhesive displayed a featureless

- amorphous phase, indicating complete monomer consumption and absence of residual
- 2 crystallinity. Meanwhile, the Raman peak located at 513 cm<sup>-1</sup> (characteristic of the -S-S- bond)
- 3 splits into two distinct peaks at 521 and 527 cm<sup>-1</sup> (Fig. 3d), indicating the successful ring-
- 4 opening polymerization of the disulfide five-membered carbocycle.

# 3.2 Underwater adhesion properties

5

6

7

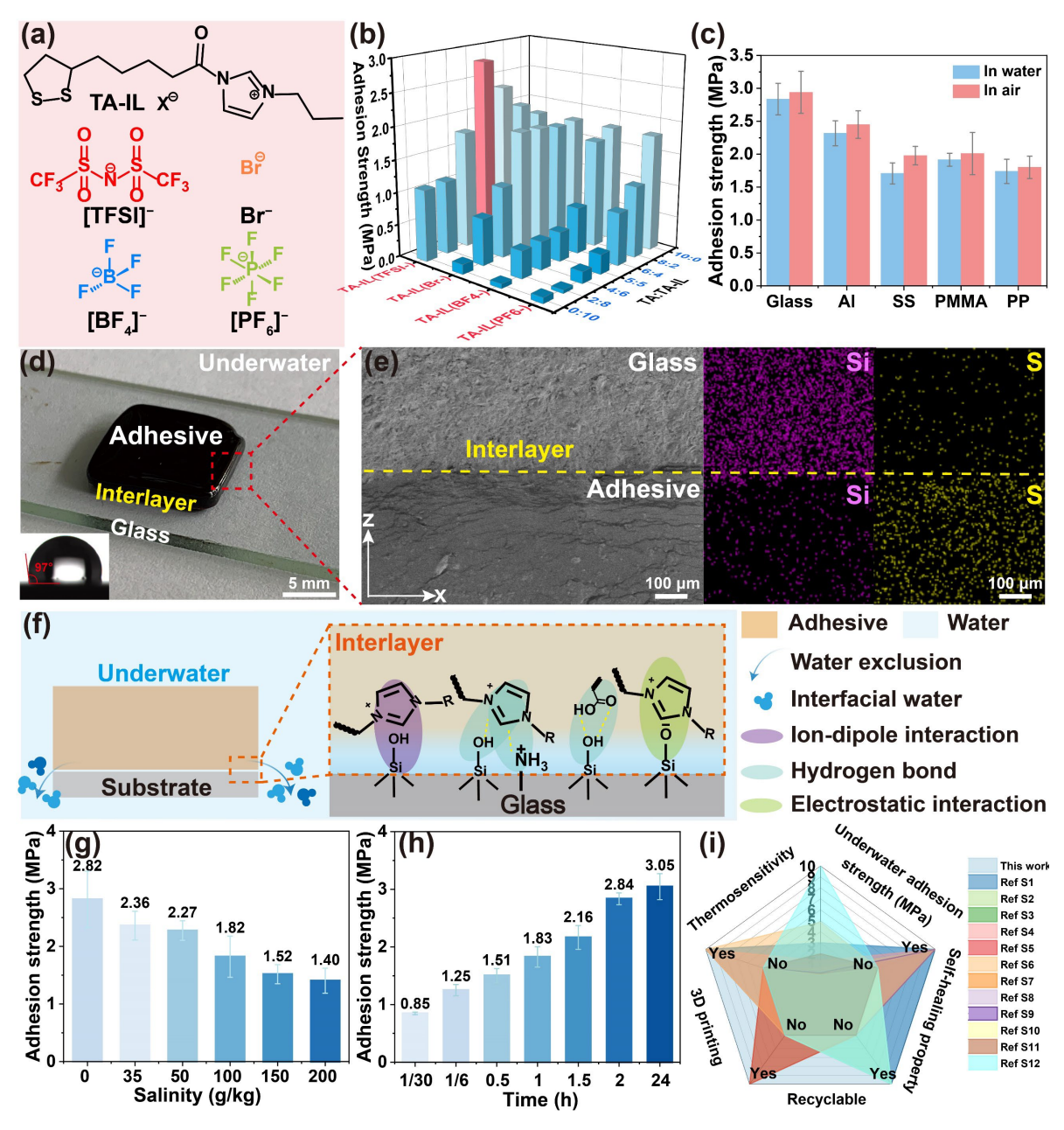


**Fig. 4.** (a) Preparation of TA-IL with different ligands; (b) Orthogonal experimental study of the PTIL adhesives; (c) Adhesion strength on different substrates; (d) Digital photographs of PTIL1 adhesives adhered to glass surfaces under water, (e) Cross-sectional SEM images and

- 1 EDS elemental distributions; (f) Schematic representation of interfacial interactions and
- 2 removal of the hydrated layer; (g) Summarization of underwater adhesion strengths of the
- 3 PTIL1 adhesives in different brines; (h) Adhesion strength of the PTIL1 adhesive on glass
- 4 slides at different curing time; (i) Reported radar charts of the underwater adhesives and the
- 5 PTIL1 adhesive.
- 6 In order to prepare an ideal PTIL adhesive for underwater adhesion, a systematic orthogonal
- 7 experimental design (in total 25 formulations) was implemented. The 25-sample orthogonal
- 8 array was constructed to assess the synergistic effects of two independent variables — anionic
- 9 ligand chemistry (Br<sup>-</sup>, TFSI<sup>-</sup>, PF<sub>6</sub><sup>-</sup> and BF<sub>4</sub><sup>-</sup>) and component ratio (TA: TA-IL) — on the
- adhesion strength of PTIL adhesives (Fig. 4a and 4b). Using standardized glass substrates 10
- 11
  - $(100 \times 26 \times 2 \text{ mm}^3)$  as the adhesion matrix, the underwater adhesion properties of the PTIL
- 12 adhesive were assessed through lap shear tests. Two glass slides were immersed in deionized
- water ( $\approx 20$  °C) with PTIL adhesive placed in between, creating an adhesive joint. All as-13
- 14 prepared samples were characterized via a lap shear testing machine. As shown in Fig. 4b, the
- maximum underwater adhesion strength exhibited significant ligand-dependent behavior, 15
- following the hierarchical order: PTIL (TFSI<sup>-</sup>) > PTIL (Br<sup>-</sup>) > PTIL (BF<sub>4</sub><sup>-</sup>) > PTIL (PF<sub>6</sub><sup>-</sup>). 16
- 17 Among the 25 formulations, PTIL1 adhesive (with TFSI<sup>-</sup> and TA: TA-IL = 5:5) achieved the
- highest adhesion strength of 3.31 MPa. PTIL1 adhesive can rapidly adhere to 2.5 kg stainless 18
- 19 steel underwater (Video S1).
- 20 Although the adhesives contain polar functional groups, their molecular design incorporates
- 21 multiple hydrophobic components that synergistically expel interfacial water. Specifically, the
- 22 polysulfide backbone (-S-S-) is intrinsically hydrophobic. In addition, the anionic ligands in
- TA-IL exhibit distinct hydrophobicity, following the order  $TFSI^- > PF_6^- > BF_4^- > Br^-$ , where 23
- 24 Br is hydrophilic while the other three anions are strongly hydrophobic. When paired with
- imidazolium cations, these hydrophobic anions significantly enhance the overall 25
- hydrophobicity of the ion-pair units. This effect effectively counterbalances the presence of 26

polar functional groups, suppressing their hydration tendency and reinforcing the expulsion of water molecules from the interface. Therefore, the efficient water removal originates from the cooperative contribution of the hydrophobic polysulfide backbone and the hydrophobic ionpair units, which together establish a robust water-repellent interfacial environment. To further investigate the structural performance, the interfacial bonding morphology between this PTIL adhesive and glass substrates was systematically characterized through macro photography and scanning electron microscopy (SEM). The PTIL1 adhesive maintained intimate interfacial contact with the substrate, exhibiting no visible cracks or structural defects (Fig. 4d). Notably, the adhesive demonstrated structural integrity retention during underwater immersion, with no mid-layer deformation observed. SEM observation was repeated three times independently, yielding similar results with consistency (Fig. S11). In addition, the energy-dispersive X-ray spectroscopy (EDS) elemental mapping further revealed the uniform distribution of S (the signature element of PTIL1 adhesive) and Si (the signature element of glass slides) across the adhesive interface at the microstructural level, with no elemental segregation (Fig. 4e). Removing the interfacial liquid layer and effectively bonding to the target surface is crucial for achieving adhesion in liquid environments. The water contact angle on the PTIL adhesive surface exceeds 90°, which means that the hydrophobic mechanism dominates the interfacial dehydration (Fig. S12). The adhesion performance of the PTIL1 adhesive was systematically evaluated across various substrates (Fig. S13). The adhesive demonstrated robust adhesion strengths in both air and underwater environments, with values consistently exceeding 1.7 MPa on all tested substrates (Glass, Al, SS, PMMA, and PP), highlighting its versatile and reliable bonding capability (Fig. 4c). Fig. 4f and Fig. S14 illustrate the underwater adhesion mechanism of PTIL1 adhesives on different matrices, which can be rationalized as follows. i) Diverse substrate groups (glass: -OH, -NH<sub>3</sub>+, -O<sup>-</sup>; PMMA: aliphatic polar; SS: Fe<sup>3+</sup>; aluminum: Al<sup>3+</sup>; PP: aliphatic non-polar)

1

2

3

4

5

6

7

8

9

10

11

12

13

14

15

16

17

18

19

20

21

22

23

24

combine with multiple bonding sites on PTIL1 to form interfacial interactions (Van der Waals 1 2 forces, hydrogen bonds, electrostatic/dipole-dipole/ion-dipole interactions), establishing 3 robust interfacial bonds. ii) The PTIL1 network is reinforced by abundant covalent/non-4 covalent bonds (i.e., hydrogen bonds, metal coordination, electrostatic interactions), significantly enhancing mechanical strength. iii) The inherent hydrophobicity of the PTIL1 5 6 adhesive repels interfacial water and preserves interfacial interactions. 7 Given the non-static marine environment represents the most demanding operational condition for adhesives, temperature fluctuations, hydraulic pressure variations, and seawater erosion 8 9 profoundly compromise adhesion integrity. Crucially, high ionic concentrations impede interfacial bonding and accelerate adhesion deterioration. The underwater adhesion of PTIL1 10 adhesive in brine with salinity range of 35–200 g kg<sup>-1</sup> was therefore tested (Fig. 4g). Lap shear 11 12 tests on identical adhesive/glass joints revealed progressively weaker underwater adhesion in saline solutions versus deionized water. Adhesion strengths measured 2.36 MPa (35 g kg<sup>-1</sup>), 13 2.27 MPa (50 g kg<sup>-1</sup>), 1.82 MPa (100 g kg<sup>-1</sup>), 1.52 MPa (150 g kg<sup>-1</sup>), and 1.40 MPa (200 g 14 kg<sup>-1</sup>). Notably, a robust adhesion strength of 1.40 MPa was maintained even at 200 g kg<sup>-1</sup> 15 16 salinity. The adhesion strength of PTIL1 adhesives demonstrates an inverse relationship with 17 salinity levels. This performance degradation primarily results from salt ions disrupting the 18 electrostatic interactions that govern adhesive forces. The PTIL1 adhesives contain both imidazolium cations and carboxyl groups, which enable interfacial adhesion through a 19 20 combination of electrostatic interactions and hydrogen bonding. In saline environments, 21 increasing ionic strength compresses the Debye length, thereby enhancing charge screening and reducing the effective electrostatic attraction at the interface[78, 79]. This explanation 22 23 aligns with the classic DLVO theory, which predicts that electrolyte-induced screening weakens surface interactions. Specifically, when ionic concentrations in the aqueous 24 environment exceed optimal thresholds, the PTIL1's adhesive capability becomes significantly 25

compromised. The swelling behavior of the PTIL1 adhesive under varying salinity and osmotic pressure was further assessed (Fig. S15). As showing in Fig. S16, the black and red dashed lines correspond to the osmotic equilibrium and specific osmotic pressure of seawater, respectively. In contrast to conventional hydrogels and polyelectrolyte systems that exhibit substantial swelling, the PTIL1 adhesives showed negligible structural deformation, with swelling ratios decreasing moderately from 5.07% to 2.51% as salinity increased. This antiswelling behavior originates from hydrophobic carbon chains and fluorinated moieties that dominate water resistance mechanisms. Collectively, these results show that PTIL1 adhesives have high underwater strength and good resistance to swelling (anti-deformation) over a wide range of salinities, highlighting its potential for application in challenging marine environments. Since the immediacy and durability of adhesives are also key considerations in their practical applications, therefore, the underwater curing was quantitatively assessed. As evident in Fig. 4h, the adhesion strength demonstrates a clear positive correlation with curing duration, suggesting that extended curing times facilitate more complete bond formation. Notably, the PTIL1 adhesive achieved 2.84 MPa after only 2 h of underwater curing, which was comparable to the peak strength (3.05 MPa) obtained after 24 h. Long-term stability was evaluated through continuous immersion of adhesive/glass joints in deionized water over 180 days, with lap shear strength measured at 15-day intervals. Although a slight decline in adhesion performance occurred over time, the adhesive retained a strength of 1.7 MPa after 180 days of continuous immersion, indicating excellent long-term underwater stability (Fig. S17). These results reveal instant, strong, durable, and long-lasting underwater bonding of such designed adhesives on various material surfaces and under different water conditions.

#### 3.3 Switchable and repeatable adhesion properties

1

2

3

4

5

6

7

8

9

10

11

12

13

14

15

16

17

18

19

20

21

22

23

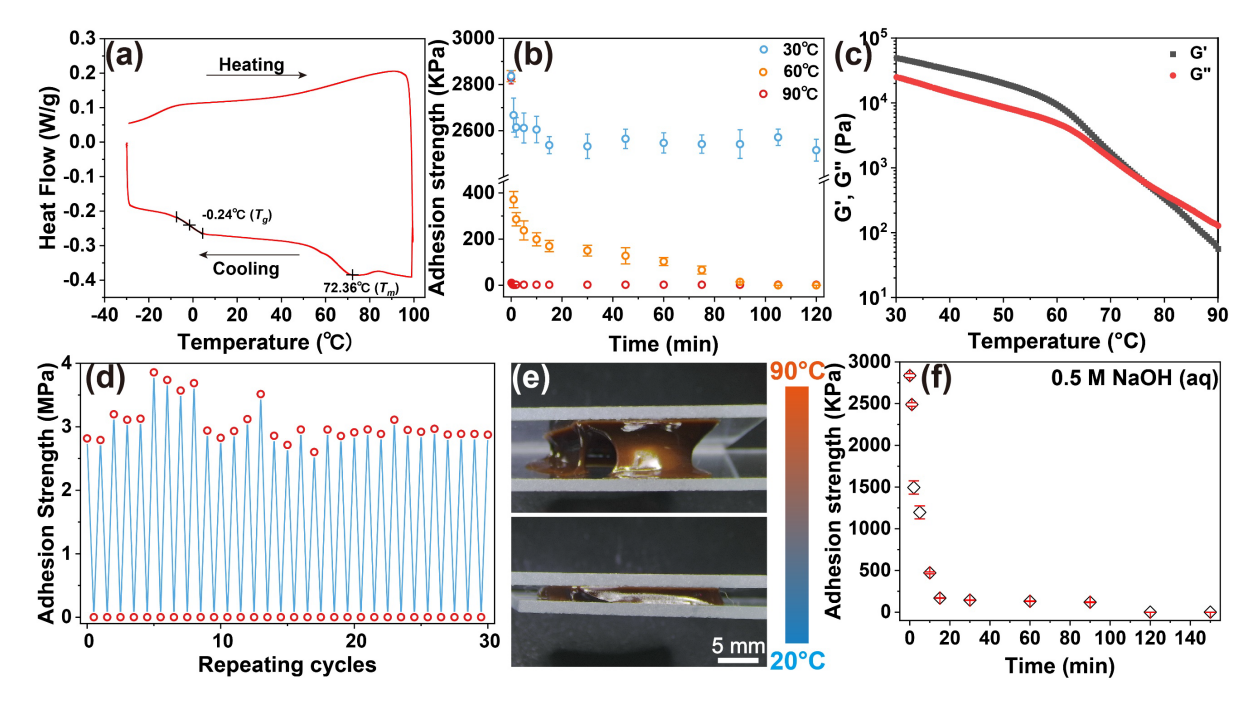


**Fig. 5.** (a) DSC curves of PTIL1 adhesive; changes of (b) underwater adhesion strengths and (c) modulus over time at different temperatures; (d) reversible underwater and repeatable adhesion upon alternating heating and cooling; (e) digital photographs of the PTIL1 adhesives heated up to 80 °C (upper) and at room temperature (bottom); (f) adhesion strength of the PTIL1 adhesives in NaOH solution with time.

From literatures, the thermos-responsiveness of dithiolane rings is well-established [80, 81], where the moderate bond dissociation energy of dynamic disulfide bonds (~268 kJ/mol) enables reversible cleavage and reformation under thermal stimuli. For PTIL1 adhesive, critical thermal transitions were quantified via DSC, revealing a glass transition temperature of -0.24 °C and melting point of 72.36 °C (**Fig. 5a**). To systematically evaluate temperature-dependent adhesive performance, lap-shear tests were conducted across three water temperature regimes (30, 60, and 90 °C) (**Fig. 5b**). At 30 °C, the adhesive strength of the PTIL1 adhesive dropped to 2500 kPa in 20 minutes, maintaining this strength for the remaining 100 minutes. Pronounced thermal degradation occurred at elevated temperatures: at 60 °C, the adhesive strength dropped from 2890 kPa to 200 kPa within the 20 minutes, culminating in cohesive failure after 90 minutes of immersion. At 90 °C, the PTIL1 adhesive instantly lost cohesive integrity (< 100 kPa), indicating phase transition to a fluid state. Notably, the

1 adhesive's melting point at 72.36 °C falls within the temperature range of 60 °C to 90 °C. 2 Therefore, when ambient temperature exceeds the melting point, PTIL1 adhesive completely 3 melts, undergoing liquefaction that disrupts cohesive networks and eliminates adhesive 4 functionality (Video S2). 5 Dynamic rheological tests were performed to investigate the deformation and flow behavior of the PTIL1 adhesive. The temperature dependence of the storage and loss moduli (G' and 6 7 G") were measured to evaluate its viscoelastic properties. G' represents the stored deformation energy, and G" represents the deformation energy lost due to internal friction during the shear 8 9 test. The PTIL1 adhesive exhibits a solid-like character with a high storage modulus (G' > G'') at room temperature, ensuring strong adhesion. Upon heating above a critical temperature 10 (~72 °C), a dramatic decrease in moduli over three orders of magnitude is observed, 11 12 accompanied by a crossover where G' surpasses G', indicating a transition to a fluid-like, 13 dissipative state. This thermal-induced abrupt softening directly facilitates the straightforward realization of thermal dissociation. This transition is attributed to the thermally reversible 14 cleavage of disulfide bonds: upon heating, the S–S bonds dissociate and the network topology 15 is reorganized, consistent with the rapid adhesive failure observed at 90 °C (Fig. 5c). 16 17 Furthermore, frequency scan (Fig. S18a) corroborates its solid-state behavior under quasistatic conditions (G' > G'' across the entire measurement frequency range), ensuring robust 18 19 bonding stability. Strain scans (Fig. S18b) confirm the strain yield response, wherein its 20 microstructure yields under large deformations, enabling mechanically triggered delamination. 21 Leveraging this thermal debonding mechanism, the reusability and reversibility of the adhesive was assessed through thermal cycling experiments. In 30 cycles of heat-triggered 22 debonding-room temperature re-adhesion, the adhesion strength always remained near the 23

initial level, fully proving the reliability and durability of the dynamic disulfide bond network

to give the PTIL1 adhesive repeated adhesion (Fig. 5d). Periodic modulation of adhesion

24

strength during thermal cycling confirmed robust thermally switchable adhesion. As shown in Fig. 5e, when heated above its melting point, the PTIL1 adhesive undergoes progressive disruption of its disulfide and hydrogen bonds, causing abrupt cohesive strength loss, fluidization, and bonding failure. In addition to thermal debonding, the PTIL1 adhesive can also be effectively debonded by immersion in an aqueous NaOH solution. Experimentally, complementary alkaline debonding was achieved by immersion in 0.5 M NaOH, with adhesive properties diminishing within 20 minutes and complete debonding occurring within 2 h. Collectively, PTIL1 adhesive features thermally and chemically (alkaline) triggered debonding mechanisms, governed by reversible disulfide bond dynamics, thereby enabling controllable detachment and robust repeatable adhesion for advanced smart adhesive systems.

## 3.4 Cohesive and Self-Healing properties of PTIL1 adhesives

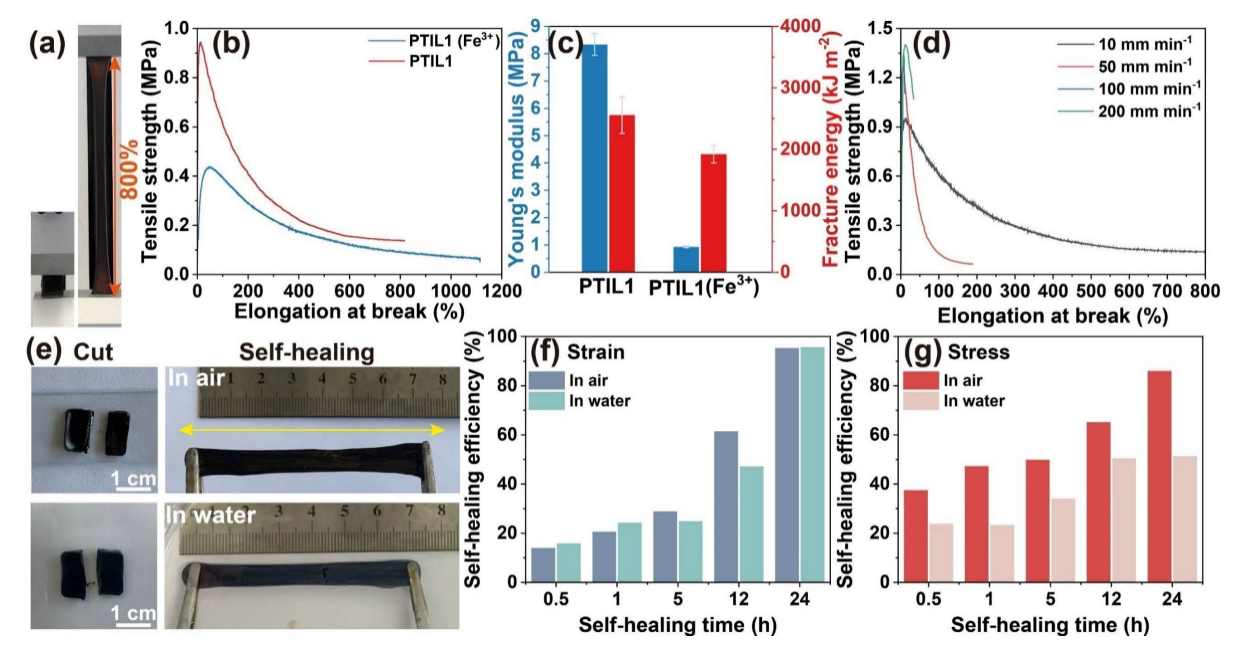


**Fig. 6.** (a) Tensile test setup and specimens; (b) Tensile stress-strain curves and (c) Summary of the mechanical properties of the PTIL1 adhesive; (d) Tensile stress-strain curves at different tensile rates; (e) Digital photographs of the PTIL1 adhesive before and after self-healing; (g) and (f) Self-healing efficiency at different self-healing times.

17 Uniaxial tensile testing was conducted to evaluate the mechanical properties of the PTIL1

adhesive (Fig. 6a). Dumbbell-shaped PTIL1 adhesives  $(40 \times 10 \times 2 \text{ mm}^3)$  were prepared using 1 2 a mold. The results of tensile strength and strain-at-break tensile are summarized in Fig. 6b. Young's modulus limit and fracture energy are summarized in Fig. 6c. The effect of PTA on 3 4 the mechanical strength of the adhesive network was also systematically investigated. PTIL1 adhesives without PTA (denoted PTIL1(Fe<sup>3+</sup>)) exhibited 0.50 MPa tensile strength, whereas 5 PTA-containing adhesive achieved 0.94 MPa. Moreover, the Young's modulus and fracture 6 energy of the PTIL1 adhesive exceeded those of PTIL1(Fe<sup>3+</sup>) adhesive, confirming PTA 7 8 enhances cohesive energy through non-covalent crosslinking. In the PTIL1 adhesive network, PTA participates in electrostatic cross-linking with imidazolium cations and forms 9 10 intermolecular hydrogen bonds with TA (Fig. 6c). This mechanism was further confirmed by 11 the decrease in elongation at break with increasing stretching rate (Fig. 6d). Therefore, it can 12 be proved that adding PTA to PTIL1 adhesive can provide more cross-linking points for the adhesive network, establish hydrogen bonds and electrostatic interactions, and can dissipate 13 energy during the stretching process. The excellent mechanical strength of the obtained 14 network can be attributed to two key aspects: (i) the presence of four different dynamic 15 16 chemical bonds, including dynamic covalent disulfide bonding, hydrogen bonding, iron-17 carboxylate ligand bonding, and electrostatic cross-linking of PTA-imidazolium cations, 18 which collectively enable hierarchical energy dissipation under stress; (ii) a large number of 19 high-density cross-linking sites within the network, which leads to a compact polymer structure with reduced interchain distances, thereby allowing enhanced polymer chain 20 21 mobility and slippage during stretching. Complex aquatic environments, including surface wave impacts, plant entanglement and 22 23 animal damage, sometimes cause physical defects in underwater adhesives. These defects tend to propagate over time, ultimately compromising interfacial bonding and reducing adhesive 24 service life[82, 83]. Therefore, there is an urgent need to develop self-healing underwater 25

adhesives. The PTIL1 adhesives exhibited intrinsic self-healing in both air and aqueous environments (Fig. 6e). When two separate samples were placed in gentle contact in air and water environment, autonomous healing occurred without any external pressure. The healed PTIL1 adhesives regained sufficient mechanical integrity to withstand stretching without failure. To further evaluate the self-healing properties of the PTIL1 adhesive, no cracks were observed on the contact interface through SEM, indicating that the PTIL1 adhesive fully realized self-healing at the microscale (Fig. S19). Elemental mapping using EDS analysis revealed a uniform distribution of F, Fe, P, and S within the healed zone, confirming microstructural-level recovery. High healing efficiency of the PTIL1 adhesive was observed both in air and underwater (Fig. 6f and 6g). The self-healing efficiency was quantitatively evaluated. After self-healing underwater, the PTIL1 adhesive regained 51.2% of its original stress and 95.6% of its original strain, respectively. After self-healing in air, the PTIL1 adhesive recovered 85.9% of the original stress and 95.2% of the original strain, respectively. More importantly, the adhesive exhibited identical recovery rates (62.3% in stress, 26.7% in strain) in simulated seawater with a salinity of 35 g/kg, demonstrating its exceptional stability in challenging environments (Fig. S20). Additionally, the effects of different healing times on the self-healing efficiency of the PTIL1 adhesives were explored. With prolonged healing durations, the efficiency increased steadily, approaching full recovery. The PTIL1 adhesive recovered 127% and 776% of its elongation at break (original value of 814%) after 0.5 and 24 h of healing underwater, respectively. The self-healing behavior is attributed to three synergistic mechanisms (Fig. S21): (i) the amphiphilicity of TA and the hydrophobicity of TA-IL determine the hydrophobicity of the PTIL1 adhesive and repel the hydration layer on the fracture surface; (ii) four different dynamic chemical bonds, including dynamic covalent sulfur bonds, hydrogen bonds, ironcarboxylate coordination bonds and imidazole cationic electrostatic cross-links, collectively

1

2

3

4

5

6

7

8

9

10

11

12

13

14

15

16

17

18

19

20

21

22

23

24

- enable reversible network reconfiguration after breakage; (iii) TFSI moieties promote
- 2 interfacial reconnection via dipole-dipole, ion-dipole, and ion-ion interactions in aqueous
- 3 environments.

- 4 Despite the robust self-healing capabilities of PTIL1 due to multiple synergistic mechanisms,
- 5 its repair efficiency underwater remains lower than that in air. This discrepancy can be
- attributed to several factors. First, while the hydrophobicity of the binder partially repels the
- 7 hydration layer, competition from water molecules is unavoidable in an aqueous environment.
- 8 Water molecules inevitably compete with dynamic interactions such as hydrogen bonding and
- 9 Fe-carboxylate coordination, thereby impairing the reversible network reconstruction after
- 10 rupture. Second, solvation and ionic shielding effects in an aqueous environment reduce the
- effectiveness of the imidazole-like electrostatic interactions and dipole-dipole associations
- facilitated by the TFSI unit. Finally, the limited mobility of the polymer chains in water due
- to solvent resistance, interfacial confinement, and localized swelling may slow the rate of
- 14 network rearrangement. Taken together, these effects explain the reduced self-healing
- efficiency underwater relative to that in air. Together, these results demonstrate that PTIL1
- adhesives possess excellent mechanical resilience and self-healing capabilities, enabling them
- 17 to maintain structural and adhesive integrity under complex, dynamic aquatic conditions.

#### 3.5 Chemical and physical closed-loop recyclability

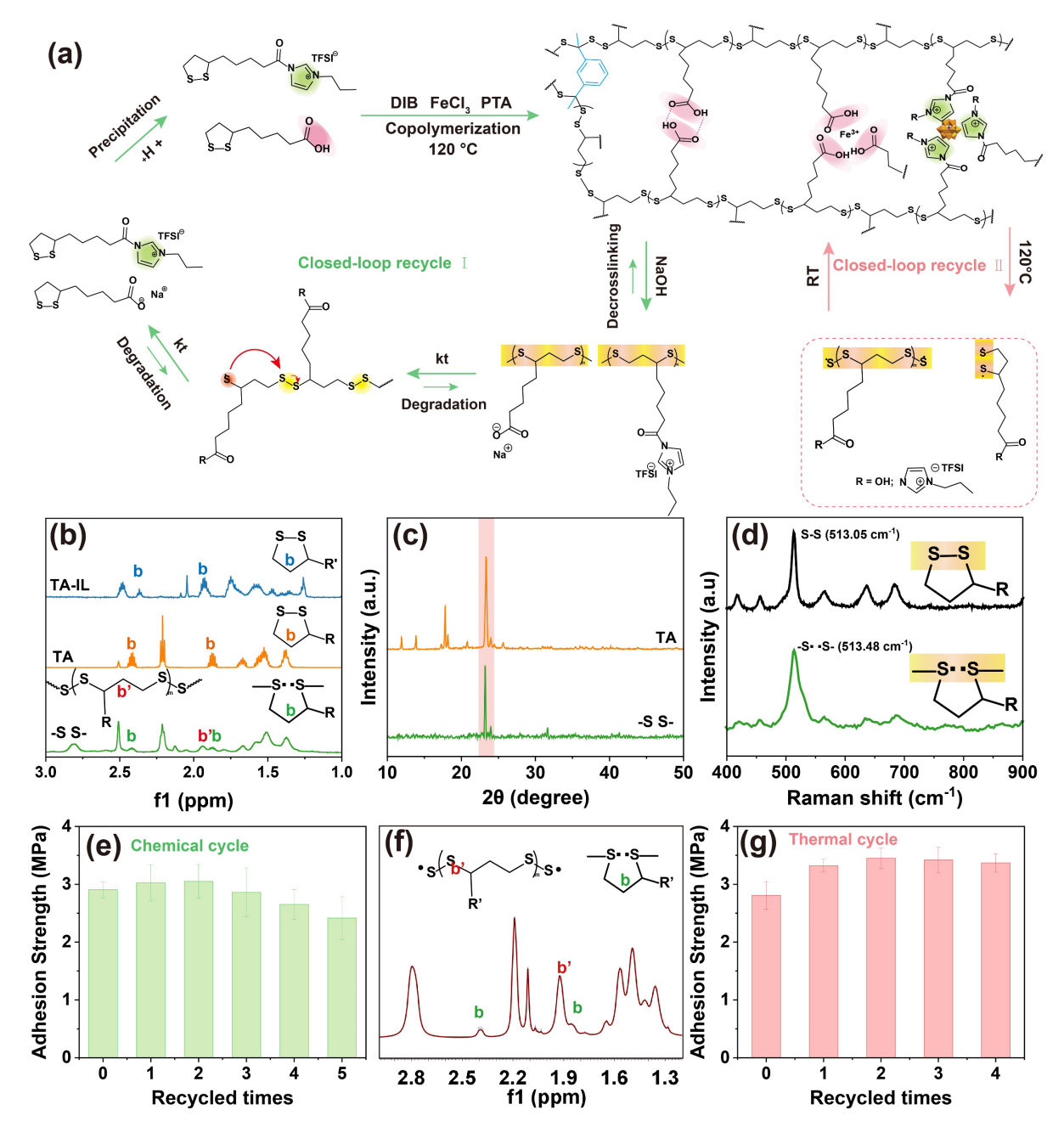


**Fig. 7.** (a) PTIL1 adhesives dual-closed-loop recycling mechanism diagram; (b) Partial <sup>1</sup>H NMR spectra of TA, TA-IL and recovered monomers by extraction-assisted acidification; (c) XRD spectra of TA and recovered monomers; (d) Comparison of the virgin feedstock and recovered monomers by direct acidification by Raman testing; (e) Variation in adhesion strength of the PTIL1 adhesives after multiple chemical cycles; (f) <sup>1</sup>H NMR spectrum of thermally recycled materials; (g) Variation in adhesion strength of the PTIL1 adhesives after multiple thermal cycles.

The development and application of underwater adhesives have added convenience to human life, posed a threat to the ecological environment, and consumed a large number of non-

renewable resources[84-87]. However, their reusability remains a critical issue that requires 1 2 further investigation. Unlike glue-type underwater adhesives (non-reusable), tape-types offer 3 reuse potential. However, their practical reuse limit remains 30 times or less. Discarded or 4 failed adhesives contribute to environmental pollution, forcing research into sustainable and 5 recyclable alternatives. This requires the development of effective recycling methods that 6 allow recycling and reprocessing while maintaining original performance. 7 The designed PTIL1 adhesives were closed-loop recycled via two distinct pathways: chemical recovery through controlled depolymerization and material regeneration through thermal 8 9 reprocessing (melting/remolding). The chemical recycling process consisted of two steps: (1) 10 Base-mediated depolymerization. Experimentally, the PTIL1 samples were immersed in 0.5 M NaOH at 25°C with stirring, producing a light-brown turbid solution (Fig. S22). The 11 12 observed turbidity originated from the limited solubility of TA-IL monomers in alkaline media, 13 and depolymerization required diluted conditions together with the activation of disulfide 14 bonds. In this context, the strong base served as a catalyst, promoting disulfide bond exchange 15 and significantly accelerating the depolymerization process. (2) Acid-induced monomer 16 recovery. The filtrate was acidified with HCl (pH = 3-4) to protonate TA monomers. Upon standing, both TA and TA-IL monomers precipitated from the solution. Residual FeCl<sub>3</sub> and 17 18 PTA were removed by repeated washing with deionized water. The loss of unrecovered monomer was attributed to the presence of spontaneous polymerization during the 19 20 acidification step, forming oligomeric colloids. A schematic illustration of the alkali-induced depolymerization process is provided in Fig. 7a. The characteristic peak of a disulfide five-21 22 membered carbocyclic ring appeared in the <sup>1</sup>H NMR spectrum (b,  $\delta = 2.40$  ppm), indicating that the method was successful in recovering the TA-R monomers (Fig. 7b and Fig. S23). 23 24 Additionally, the presence of imidazole ring signals at  $\delta = 7.86$ , 7.40, and 7.12 ppm, along with a hydroxyl proton signal at  $\delta = 12.00$  ppm, further verified the recovery of TA and TA-25

IL monomers. Based on <sup>1</sup>H NMR integration, the solid recovered was calculated to contain 1 2 10.4% polymer and 89.6% TA-R (TA and TA-IL) monomer. XRD analysis showed a sharp crystallization peak at  $\sim 23^{\circ}$  (Fig. 7c), confirming the successful recovery of the TA monomer. 3 4 The Raman spectrum also confirmed the successful recovery of TA-R monomer, with the characteristic peak of the -S-S- bond of the monomer appearing at 513.48 cm<sup>-1</sup> (Fig. 7d). 5 6 To ascertain the sustainability of the methodology, a systematic evaluation of the chemically 7 recycled PTIL1 adhesive's mechanical and underwater adhesive properties was conducted. 8 The adhesives regenerated via chemical recycling maintained tensile strength in the range of 9 0.6–0.8 MPa and exhibited high ductility (strain at break: ~800%) (Fig. S24). The recovered monomers were repolymerized to produce a closed-loop recycled PTIL adhesive. The recycled 10 11 adhesive retained excellent underwater adhesion, with its bonding strength remaining 12 relatively stable (Fig. 7e). After the fifth chemical recycling cycle, a slight decline in adhesion 13 strength was observed, potentially due to the influence of minor polymer impurities introduced during the process. Overall, these results confirm the chemical recyclability of the PTIL 14 adhesive system. 15 Compared with chemical recycling, the closed-loop thermal cycle of PTIL1 adhesives was 16 operationally more straightforward. DSC analysis showed that the PTIL1 adhesive exhibited 17 18 a distinct melting transition at 76.3 °C, which enabled the implementation of a scalable thermal 19 recycling strategy. The expired PTIL1 adhesives were thermally remolded at 80 °C for 30 20 minutes, undergoing complete solid-to-melt phase transition. After cooling the sample back to 21 room temperature, the PTIL1 adhesive was re-formed (Fig. 7a and Fig. S25). The emergence of a methylene group peak (b', chemical shift: 1.93 ppm) in the open-ring structure, observed 22 by <sup>1</sup>H NMR after thermal cycling (Fig. 7f), confirmed the reversible nature of the PTIL1 23 24 adhesive and demonstrated its potential for repeated thermal regeneration. Notably, this meltbased reprocessing strategy circumvents the intrinsic reuse limitations of tape-type adhesives 25

and offers theoretical potential for unlimited recyclability. To evaluate the sustainability of this approach, the mechanical properties and underwater adhesive performance of the PTIL1 adhesives thermal recycled were systematically characterized. The thermally cycled PTIL1 adhesive exhibited excellent mechanical integrity retention, with the maximum tensile stress remaining above 1 MPa even after four consecutive recycling cycles (Fig. S26). The thermally recycled adhesive exhibited excellent underwater bonding behavior. The successful reconstruction of the adhesive waste residue was attributed to the reversible and dynamic polymer system. Even after five recycling cycles, the adhesive's underwater shear strength remained at its original level without degradation. These results suggest that both chemical and physical closed-loop recycling strategies effectively preserve the essential viscoelastic characteristics required for practical adhesive applications.

#### 3.6 3D Printing

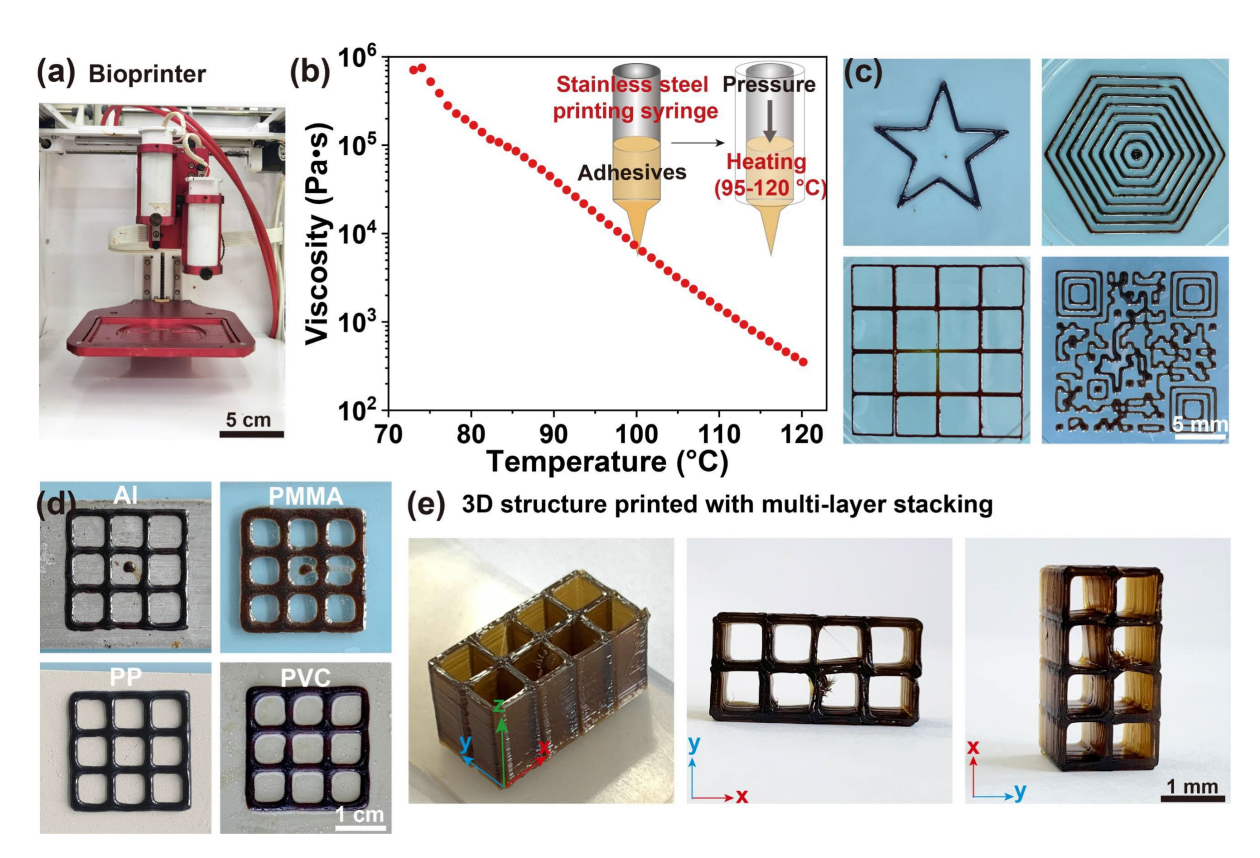


Fig. 8. (a) Photograph of Allevi 2 bioprinter; (b) Shear viscosity changes of the PTIL1 adhesives at different temperatures; (c) Digital photograph of the PTIL1 adhesive-based 3D

- printed infill pattern; (d) 3D printed models of the PTIL1 adhesives on different surfaces (from
- 2 left to right, Al, PMMA, PP, PVC); (e) 3D-printed matrices based on PTIL1 adhesives ink.
- 3 Based on reversible, temperature-dependent rheological tests, the PTIL1 adhesive
- 4 demonstrates significant potential as a high-performance heat-treatable material (10<sup>6</sup> to 10<sup>3</sup>
- 5 Pa·s across 95–120 °C, Fig. 8b), enabling precise extrusion through stainless steel nozzles of
- 6 the bioprinter (Fig. 8a). As shown in Fig. 8b, adhesive models of various sizes and geometries
- 7 were successfully fabricated via casting, without the use of organic solvents during processing.
- 8 This green manufacturing approach exhibits exceptional potential for industrial-scale
- 9 production while maintaining environmental sustainability. After multiple heating-cooling
- 10 cycles, no significant decrease in mechanical properties was detected, indicating high
- reusability of the PTIL1 adhesive (**Fig. S24**).
- 12 To further expand the processing capabilities of the PTIL1 adhesive, extrusion-based 3D
- printing was employed using an Allevi 2 bioprinter equipped with a 0.4 mm diameter nozzle.
- 14 The adhesive was printed at a temperature range of 95–120 °C, a print speed of 6 mm·s<sup>-1</sup>, and
- an extrusion pressure of 6.0 psi. Within this temperature window, precise thermal control is
- essential to maintain optimal rheological behavior and ensure strong interlayer adhesion. It
- can be successfully printed in-situ on the surfaces of Al, PMMA, PP and PVC (Fig. 8c). Due
- 18 to the adhesive's strong interfacial adhesion, the printed material adheres firmly to the
- underlying substrate. Taking the printed adhesive lattice ( $1 \times 2 \text{ cm}^2$ , 8 lattice) as an example,
- 20 fine adhesive lines were tightly deposited in a layer-by-layer manner and were printed onto
- 21 the silicone substrate (Video S3). Remarkably, the printed architectures exhibited free-
- standing 3D stability across multiple orientations, enabled by the adhesive's rapid thermos-
- reversible curing kinetics (Fig. 8d). These findings highlight the significant potential of this
- 24 adhesive for creating complex, solvent-free, stable, and adherent 3D structures.

#### 4. Conclusions

1

2

3

4

5

6

7

8

9

10

11

12

13

14

15

16

17

18

19

20

21

23

In summary, a series of underwater adhesives with switchable adhesion, recyclability, and 3D printability were developed based on TA and TA-IL through a solvent-free melt copolymerization method integrated with multiple dynamic crosslinking strategies. These systems integrated three synergistic structural design strategies: i) The ionic structure, fluorinated unit and carboxyl structure synergistically form multiple interfacial bonds to exclude interfacial water and achieve underwater adhesion. Dynamic cross-linking networks constructed from ionic liquids containing disulfide five-membered carbon rings and TA reinforce the overall network, further improve the adhesion and cohesive strength, and achieve an underwater adhesion strength up to  $2.82 \pm 0.49$  MPa. ii) The dynamic disulfide bonds exhibit temperature-responsive reversibility, enabling thermally controlled, repeatable, and switchable adhesion with capable of 30 reuse cycles. iii) The melt processing characteristics of the adhesive can accurately customize adhesive patches with complex structures through Extrusion-based 3D printing. Moreover, the adhesive's dual closed-loop chemical and physical recyclability, enabled by dynamic chemistry, lays a solid foundation for the development and sustainable reuse of environmentally friendly underwater adhesives. With all the above discovered performances, this work not only provides new ideas for synthesizing the design of the underwater adhesive design with repeatable adhesion and recyclable adhesive, but also promotes the development of multifunctionally integrated underwater adhesive systems.

## **Declaration of competing interest**

22 The authors declare no competing financial interest.

#### Acknowledgements

- 24 The authors acknowledge the financial support from the National Natural Science Foundation
- of China (Grant No. 22379133), Taishan Scholar Program of Shandong Province, China

- 1 (Grant No. tsqn201812026), Natural Science Foundation of Shandong Province, China (Grant
- 2 Nos. ZR2023MB087), Natural Science Foundation of Qingdao, China (Grant No. 23-2-1-243-
- 3 zyyd-jch).

#### Notes and references

- 5 [1] H. Fan, J.P. Gong, Bioinspired underwater adhesives, Adv. Mater. 33 (2021) 2102983.
- 6 [2] M. Vahdati, D. Hourdet, C. Creton, Soft underwater adhesives based on weak molecular interactions, Prog. Polym. Sci. 139 (2023) 101649.
- 8 [3] J. Yang, R. Bai, B. Chen, Z. Suo, Hydrogel adhesion: a supramolecular synergy of chemistry, topology, and mechanics, Adv. Funct. Mater. 30 (2019) 1901693.
- 10 [4] A. Narayanan, A. Dhinojwala, A. Joy, Design principles for creating synthetic underwater 11 adhesives, Chem. Soc. Rev. 50 (2021) 13321-13345.
- 12 [5] X. Ma, X. Zhou, J. Ding, B. Huang, P. Wang, Y. Zhao, Q. Mu, S. Zhang, C. Ren, W. Xu, Hydrogels for underwater adhesion: adhesion mechanism, design strategies and applications, J. Mater. Chem. A. 10 (2022) 11823-11853.
- 15 [6] C. Zhou, X. Song, R. Wei, S. Liu, Z. Wu, H. Chen, A conductive ionogel with Stretchability, low hysteresis and adjustable adhesion for Air/Underwater mechanosensing, Chem. Eng. J. 499 (2024) 155992.
- 18 [7] P. Huang, H. Zhang, H. Zeng, Mussel-Inspired Molecular Strategies for Fabricating 19 Functional Materials With Underwater Adhesion and Self-Healing Properties, Adv. 20 Mater. 37 (2025) 2501542.
- 21 [8] Z. Wang, X. Wan, S. Wang, Bioinspired chemical design to control interfacial wet adhesion, Chem. 9 (2023) 771-783.
- [9] M. Li, A. Mao, Q. Guan, E. Saiz, Nature-inspired adhesive systems, Chem. Soc. Rev. 53
  (2024) 8240-8305.
- [10] Y. Guo, X. Wang, L. Zhang, X. Zhou, S. Wang, L. Jiang, H. Chen, From Dry to Wet, the
  Nature Inspired Strong Attachment Surfaces and Their Medical Applications, ACS Nano.
  19 (2025) 9684-9708.
- 28 [11] S.J. Wu, X. Zhao, Bioadhesive technology platforms, Chem. Rev. 123 (2023) 14084-29 14118.
- 30 [12] Y. Kim, S.E. Kim, K.D. Park, K.M. Park, Bioadhesives and bioactive hydrogels for wound management, J. Control. Release. 379 (2025) 285-302.
- [13] P. Huang, H. Zhang, H. Zeng, Mussel-Inspired Molecular Strategies for Fabricating
  Functional Materials With Underwater Adhesion and Self-Healing Properties, Adv.
  Mater. 37 (2025) 2501542.
- [14] B. Pang, W. Li, J. Li, S. Yang, T. Sun, Q. Yu, K. Yue, W. Zhang, A Microphase
  Separation-Driven Supramolecular Tissue Adhesive with Instantaneous Dry/Wet
  Adhesion, Alcohol-Triggered Debonding, and Antibacterial Hemostasis, Adv. Mater. 37
  (2025) e2501810.
- 39 [15] Y. Chen, J. Meng, Z. Gu, X. Wan, L. Jiang, S. Wang, Bioinspired multiscale wet adhesive surfaces: structures and controlled adhesion, Adv. Funct. Mater. 30 (2019) 1905287.
- [16] M. Li, L. Shi, X. Wang, Physical mechanisms behind the wet adhesion: From amphibian toe-pad to biomimetics, Colloids Surf. B. Biointerfaces. 199 (2021) 111531.
- [17] D.A. Qureshi, S. Goffredo, Y. Kim, Y. Han, M. Guo, S. Ryu, Z. Qin, Why mussel byssal plaques are tiny yet strong in attachment, Matter. 5 (2022) 710-724.
- 45 [18] S.X. Wang, J.H. Waite, Catechol redox maintenance in mussel adhesion, Nat. Rev. Chem.

- 1 9 (2025) 159-172.
- [19] R.L. Dupont, Y. Xu, A. Borbora, X. Wang, F. Azadi, K. Havener, B. Lewis, W. Deng,
  B.W. Tan, S. Li, R. Zhang, Y. Yao, U. Manna, X. Wang, Synergistic Adhesion and Shape
  Deformation in Nanowire-Structured Liquid Crystal Elastomers, Adv. Mater. 37 (2025)
  2414695.
- [20] Y. Xu, J. Hu, X. Zhang, D. Yuan, G. Duan, Y. Li, Robust and multifunctional natural polyphenolic composites for water remediation, Mater. Horiz. 9 (2022) 2496-2517.
- 8 [21] Y. Zhang, X. Wan, X. Xu, P. Teng, S. Wang, Recent progress of tree frog toe pads inspired wet adhesive materials, BSBT. 8 (2022) 279-289.
- 10 [22] W. Qiu, Y. Huang, H. Zhu, Y. Long, Q. Zhang, S. Zhu, Unlocking the potential of supramolecular polymers with bimodal molecular weights for instant and strong underwater adhesion, Chem. Eng. J. 496 (2024) 153880.
- [23] G. Pan, F. Li, S. He, W. Li, Q. Wu, J. He, R. Ruan, Z. Xiao, J. Zhang, H. Yang, Mussel and barnacle cement proteins-inspired dual-bionic bioadhesive with repeatable wet-tissue
  adhesion, multimodal self-healing, and antibacterial capability for nonpressing
  hemostasis and promoted wound healing, Adv. Funct. Mater. 32 (2022) 2200908.
- [24] Z. Yuan, T. Wang, C. Shao, S. Yang, W. Sun, Y. Chen, Z. Peng, Z. Tong, Bioinspired
  Green Underwater Adhesive Gelatin-Tannic Acid Hydrogel With Wide Range
  Adjustable Adhesion Strength and Multiple Environmental Adaptability, Adv. Funct.
  Mater. 35 (2024) 2412950.
- [25] B. Zhang, W. Yuan, Ultra-stretchable and highly tough ionogels with underwater repeatable adhesion and anti-swelling capacity for real-time motion detection, signal transmission and electrochemical monitoring platforms, Chem. Eng. J. 487 (2024) 150508.
- [26] H. Fan, J. Wang, J.P. Gong, Barnacle cement proteins-inspired tough hydrogels with
  robust, long-lasting, and repeatable underwater adhesion, Adv. Funct. Mater. 31 (2021)
  2009334.
- 28 [27] L. Yin, A. Cholewinski, B. Zhao, Solvent-free urethane-based prepolymer as a versatile underwater adhesive material, Chem. Eng. J. 481 (2024) 148487.
- [28] X. Jiang, X. Xu, Z. Xia, D. Lin, Y. Chen, Y. Wang, D. Yu, X. Wu, H. Zeng, Simultaneous
  Segment Orientation and Anchoring for Robust Hydrogel Coating with Underwater
  Superoleophobicity, Adv. Funct. Mater. 34 (2024) 2314589.
- 133 [29] T. Nogusa, C.B. Cooper, Z. Yu, Y. Zheng, Y. Shi, Z. Bao, Tunable, reusable, and 134 recyclable perfluoropolyether periodic dynamic polymers with high underwater adhesion 135 strength, Matter. 6 (2023) 2439-2453.
- [30] M. Gao, H. Wu, R. Plamthottam, Z. Xie, Y. Liu, J. Hu, S. Wu, L. Wu, X. He, Q. Pei, Skin
  temperature-triggered, debonding-on-demand sticker for a self-powered
  mechanosensitive communication system, Matter. 4 (2021) 1962-1974.
- 39 [31] Y. Hou, Y. Li, Y. Li, D. Li, T. Guo, X. Deng, H. Zhang, C. Xie, X. Lu, Tuning water-40 resistant networks in mussel-inspired hydrogels for robust wet tissue and bioelectronic 41 adhesion, ACS Nano. 17 (2023) 2745-2760.
- 42 [32] Q. Zhu, R. Li, Y. Yan, Y. Huang, H. Su, Y. Dong, X. Pan, W. Sun, X. Wang, H. Meng, 43 R. Wang, H. Ouyang, Y. Hong, Sustainable Snail-Inspired Bio-Based Adhesives with 44 Ultra-High Adhesion, Adv. Funct. Mater. 34 (2024) 2402734.
- [33] H. Wang, X. Shi, Y. Xie, S. Gao, Y. Dai, C. Lai, D. Zhang, C. Wang, Z. Guo, F. Chu, A
  furan-containing biomimetic multiphase structure for strong and supertough sustainable
  adhesives, Cell Rep. Phys. Sci. 4 (2023) 101374.
- 48 [34] H.-M. Wang, T.-Q. Yuan, G.-Y. Song, R.-C. Sun, Advanced and versatile lignin-derived 49 biodegradable composite film materials toward a sustainable world, Green Chem. 23 50 (2021) 3790-3817.

- 1 [35] W. Guo, M. Huang, L. Cui, G. Gao, Q. Zhang, X. Liu, Water-resistant adhesive tackified 2 by dynamic adhesion factor of nucleotide, Chem. Eng. J. 498 (2024) 155710.
- 3 [36] Z.-H. Wang, B.-W. Liu, F.-R. Zeng, X.-C. Lin, J.-Y. Zhang, X.-L. Wang, Y.-Z. Wang, H.-B. Zhao, Fully recyclable multifunctional adhesive with high durability, transparency, flame retardancy, and harsh-environment resistance, Sci. Adv. 8 (2022) eadd8527.
- 6 [37] B. Cheng, J. Yu, T. Arisawa, K. Hayashi, J.J. Richardson, Y. Shibuta, H. Ejima, Ultrastrong underwater adhesion on diverse substrates using non-canonical phenolic groups, Nat Commun. 13 (2022) 1892.
- 9 [38] R. Ou, S. Wang, J. Li, Z. Li, L. Yu, Z. Wang, P. Murto, X. Xu, Robust, Switchable and 10 Printable Underwater Adhesives Based on a Temperature-Deactivated Design, Adv. 11 Funct. Mater. 35 (2024) 2416043.
- 12 [39] R. Yang, L. Tan, Z. Pan, L. Tian, T. Zhang, B. Zhao, F. Song, Y. Zhou, M. Zhang, High 13 strength, self-activating ability and fast adhesion of polyurethane adhesives based on 14 rosin structure in different environments, Mater. Horiz. 12 (2025) 1913-1921.
- 15 [40] P. Tan, W. Gu, Y. Zou, X. Song, Z. Huang, J. Liu, I.M. Lei, Harnessing dynamic covalent 16 chemistry in sustainable biomass-based polymers: Synthesis, dynamic functionalities and 17 potential of dithiolane-containing supramolecular polymers, Prog. Polym. Sci. 160 (2025) 18 101920.
- 19 [41] M. Huang, L. Liu, W. Guo, L. Cui, G. Gao, Q. Zhang, X. Liu, Nucleotide-Tackified 20 Degradable and Closed-Loop Recyclable Underwater Adhesive, Adv. Funct. Mater. 35 21 (2024) 2413542.
- [42] S. Zhang, T. Liu, C. Hao, L. Wang, J. Han, H. Liu, J. Zhang, Preparation of a lignin-based
  vitrimer material and its potential use for recoverable adhesives, Green Chem. 20 (2018)
  2995-3000.
- 25 [43] S. Zhao, M.M. Abu-Omar, Catechol-Mediated Glycidylation toward Epoxy Vitrimers/Polymers with Tunable Properties, Macromolecules. 52 (2019) 3646-3654.
- [44] Y. Fu, S. Chen, X. Chen, H. Zheng, X. Yan, Z. Liu, M. Wang, L. Liu, A Hierarchical
  Energy Dissipated Structure Enabled Strong, Ultra-Tough, and Sustainable Adhesives,
  Adv. Funct. Mater. 34 (2024) 2314561.
- [45] S. Das, S. Samitsu, Y. Nakamura, Y. Yamauchi, D. Payra, K. Kato, M. Naito, Thermoresettable cross-linked polymers for reusable/removable adhesives, Polym. Chem. 9
  (2018) 5559-5565.
- [46] L.M. Sridhar, M.O. Oster, D.E. Herr, J.B.D. Gregg, J.A. Wilson, A.T. Slark, Re-usable
  thermally reversible crosslinked adhesives from robust polyester and poly(ester urethane)
  Diels-Alder networks, Green Chem. 22 (2020) 8669-8679.
- [47] Z.-H. Zhao, P.-C. Zhao, Y. Zhao, J.-L. Zuo, C.-H. Li, An underwater long-term strong
  adhesive based on boronic esters with enhanced hydrolytic stability, Adv. Funct. Mater.
  32 (2022) 2201959.
- [48] Z. Zhou, X. Su, J. Liu, R. Liu, Synthesis of Vanillin-Based Polyimine Vitrimers with
  Excellent Reprocessability, Fast Chemical Degradability, and Adhesion, ACS Appl.
  Polym. Mater. 2 (2020) 5716-5725.
- 42 [49] Z. Lei, H. Chen, S. Huang, L.J. Wayment, Q. Xu, W. Zhang, New Advances in Covalent Network Polymers via Dynamic Covalent Chemistry, Chem. Rev. 124 (2024) 7829-7906.
- [50] N. Zheng, Y. Xu, Q. Zhao, T. Xie, Dynamic Covalent Polymer Networks: A Molecular
  Platform for Designing Functions beyond Chemical Recycling and Self-Healing, Chem.
  Rev. 121 (2021) 1716-1745.
- [51] Q. Li, S. Zheng, Z. Liu, W. Li, X. Wang, Q. Cao, F. Yan, Strong, Spontaneous, and Self Healing Poly(Ionic Liquid) Elastomer Underwater Adhesive with Borate Ester Dynamic
  Crosslinking, Adv. Mater. 36 (2024) e2413901.
- 50 [52] Y. Lai, X. Kuang, P. Zhu, M. Huang, X. Dong, D. Wang, Colorless, Transparent, Robust,

- and Fast Scratch-Self-Healing Elastomers via a Phase-Locked Dynamic Bonds Design, Adv. Mater. 30 (2018) 1802556.
- 3 [53] Y. Yan, J. Huang, X. Qiu, D. Zhuang, H. Liu, C. Huang, X. Wu, X. Cui, A strong underwater adhesive that totally cured in water, Chem. Eng. J. 431 (2022) 133460.
- 5 [54] X. Zhu, C. Wei, H. Chen, C. Zhang, H. Peng, D. Wang, J. Yuan, J.H. Waite, Q. Zhao, A cation-methylene-phenyl sequence encodes programmable poly(Ionic Liquid) coacervation and robust underwater adhesion, Adv. Funct. Mater. 32 (2022) 2105464.
- [55] Q. Peng, J. Chen, T. Wang, L. Gong, X. Peng, M. Wu, Y. Ma, F. Wu, D. Yang, H. Zhang,
  H. Zeng, Coacervation-driven instant paintable underwater adhesives with tunable optical and electrochromic properties, J. Mater. Chem. A. 9 (2021) 12988-13000.
- 11 [56] X. Zhu, C. Wei, F. Zhang, Q. Tang, Q. Zhao, A robust salty water schesive by counterion exchange induced coacervate, Macromol. Rapid Commun. 40 (2019) 1800758.
- [57] D.W. Kim, K.-I. Song, D. Seong, Y.S. Lee, S. Baik, J.H. Song, H.J. Lee, D. Son, C. Pang,
  Electrostatic-mechanical synergistic in situ multiscale tissue adhesion for sustainable
  residue-free bioelectronics interfaces, Adv. Mater. 34 (2022) 2105338.

- [58] P. Rao, T.L. Sun, L. Chen, R. Takahashi, G. Shinohara, H. Guo, D.R. King, T. Kurokawa, J.P. Gong, Tough hydrogels with fast, strong, and reversible underwater adhesion based on a multiscale design, Adv. Mater. 30 (2018) 1801884.
- 19 [59] S.J. Wu, J. Wu, S.J. Kaser, H. Roh, R.D. Shiferaw, H. Yuk, X. Zhao, A 3D printable tissue adhesive, Nat Commun. 15 (2024) 1215.
- [60] L. Zhang, H. Du, X. Sun, F. Cheng, W. Lee, J. Li, G. Dai, N.X. Fang, Y. Liu, 3D printing
  of interpenetrating network flexible hydrogels with enhancement of adhesiveness, ACS
  Appl. Mater. Interfaces. 15 (2023) 41892-41905.
- 24 [61] Y. Deng, Q. Zhang, B.L. Feringa, H. Tian, D.H. Qu, Toughening a self-healable supramolecular polymer by Ionic cluster-enhanced Iron-carboxylate complexes, Angew. Chem. Int. Edit. 59 (2020) 5278-5283.
- [62] C. Cai, S. Wu, Y. Zhang, F. Li, Z. Tan, S. Dong, Poly(thioctic acid): from bottom-up self-assembly to 3D-fused deposition modeling printing, Adv. Sci. 9 (2022) 2203630.
- [63] J.-Q. Wang, X. Ling, H.-J. Wang, F.-E. Chen, α-Lipoic acid chemistry: the past 70 years,
  RSC Adv. 13 (2023) 36346-36363.
- [64] Z. Li, Z. Zhang, X. Ji, W. Wang, M. Xu, H. Cui, C. Du, L. Wang, Lipoic acid-based stable
  underwater adhesive with repeatable adhesion and recyclability, Chem. Eng. J. 512 (2025)
  162309.
- [65] Y. Li, Y. Shen, H. Liu, Z. Sun, J. Yu, J. Li, S. Liu, Biomass-Driven Composites with
  Integrated Hydrophobicity, mechanical Resilience, and enhanced conductivity for
  underwater sensing and adhesion, Chem. Eng. J. 511 (2025) 162054.
- [66] H. Huang, R. Xu, Y. Fang, Y. Weng, Q. Chen, Z. Wang, H. Liu, X. Fan, Biodegradable
  underwater tissue adhesive enabled by dynamic poly(thioctic acid) network, Chem. Eng.
  J. 489 (2024) 151352.
- [67] H. Guo, W. Zhang, Z. Jia, P. Wang, Q. Shao, H. Shen, J. Li, Q. Chen, B. Chi, A
  Biodegradable Supramolecular Adhesive with Robust Instant Wet Adhesion for Urgent
  Hemostasis and Wound Repair, Adv. Funct. Mater. 34 (2024) 2401529.
- [68] J. Gao, Q. Zhang, B. Wu, X. Gao, Z. Liu, H. Yang, J. Yuan, J. Huang, Mussel-Inspired,
  Underwater Self-Healing Ionoelastomers Based on α-Lipoic Acid for Iontronics, Small.
  19 (2023) 2207334.
- [69] Q. Zhang, D.-H. Qu, B.L. Feringa, H. Tian, Disulfide-mediated reversible polymerization
  toward intrinsically dynamic smart materials, J. Am. Chem. Soc. 144 (2022) 2022-2033.
- 48 [70] G. Yao, M. Gao, Q. Zhang, X. Tan, C. Cai, S. Dong, Electric-Field Regulation of Adhesion/De-Adhesion/Release Capacity of Transparent and Electrochromic Adhesive, Adv. Mater. 37 (2025) 2500648.

- 1 [71] N. Jarach, M. Cohen, R. Gitt, H. Dodiuk, S. Kenig, S. Magdassi, Untying the Knot: A 2 Fully Recyclable, Solvent-Free, Wide-Spectral Photocurable Thermoset Adhesive, Adv. 3 Mater. 37 (2025) 2502040.
- 4 [72] J. Zhang, Z. Chen, Y. Zhang, S. Dong, Y. Chen, S. Zhang, Poly(ionic liquid)s containing alkoxy chains and bis(trifluoromethanesulfonyl)imide anions as highly adhesive materials, Adv. Mater. 33 (2021) 2100962.
- [73] R. Zhou, Y. Jin, W. Zeng, H. Jin, Y. Li, J. Mei, J. Liu, Janus Hydrophobic Structural Gel
  with Asymmetric Adhesion in Air/Underwater for Reliable Mechanosensing, Adv. Funct.
  Mater. 34 (2024) 2316687.
- 10 [74] S. Wang, R. Ou, J. Li, K. Jin, L. Yu, P. Murto, Z. Wang, X. Xu, Deformation-Resistant Underwater Adhesion in a Wide Salinity Range, Small. 20 (2024) 2403350.
- 12 [75] Y. Hu, K. Liu, P. Wu, Strong Underwater Supramolecular Adhesives via Fluorinated Ionic Liquids, Adv. Funct. Mater. 35 (2025) 2502134.
- 14 [76] R. Xue, N. Zhou, S. Yin, Z. Qian, Z. Dai, Y. Xiong, All-polymer dynamical ionogel-like 15 materials with benzyl-mediated ultra-strong adhesion for flexible sensor application, 16 Chem. Eng. J. 465 (2023) 143072.
- [77] Q. Li, S. Zheng, Z. Liu, W. Li, X. Wang, Q. Cao, F. Yan, Strong, Spontaneous, and Self Healing Poly(Ionic Liquid) Elastomer Underwater Adhesive with Borate Ester Dynamic
  Crosslinking, Adv. Mater. 36 (2024) 2413901.
- 20 [78] B. Derjaguin, L. Landau, Theory of the stability of strongly charged lyophobic sols and of the adhesion of strongly charged particles in solutions of electrolytes, Prog. Surf. Sci. 43 (1993) 30-59.
- 23 [79] J.A.V. Butler, Theory of the Stability of Lyophobic Colloids, Nature. 162 (1948) 315-24 316.
- 25 [80] D. Pei, S. Yu, P. Liu, Y. Wu, X. Zhang, Y. Chen, M. Li, C. Li, Reversible wet-adhesive 26 and self-healing conductive composite elastomer of liquid metal, Adv. Funct. Mater. 32 27 (2022) 2204257.
- 28 [81] Q. Zhang, C.-Y. Shi, D.-H. Qu, Y.-T. Long, B.L. Feringa, H. Tian, Exploring a naturally tailored small molecule for stretchable, self-healing, and adhesive supramolecular polymers, Sci. Adv. 4 (2018) eaat8192.
- 11 [82] L. Xu, Z. Huang, Z. Deng, Z. Du, T.L. Sun, Z.-H. Guo, K. Yue, A transparent, highly 12 stretchable, solvent-resistant, recyclable multifunctional ionogel with underwater self-13 healing and adhesion for reliable strain sensors, Adv. Mater. 33 (2021) 2105306.
- [83] S. Wang, J. Li, S. Li, X. Wu, C. Guo, L. Yu, P. Murto, Z. Wang, X. Xu, Self-Contained
  Underwater Adhesion and Informational Labeling Enabled by Arene-Functionalized
  Polymeric Ionogels, Adv. Funct. Mater. 33 (2023) 2306814.
- [84] Y. Zhao, F. Wang, J. Liu, D. Gan, B. Lei, J. Shao, W. Wang, Q. Wang, X. Dong,
  Underwater Self-Healing and Recyclable Ionogel Sensor for Physiological Signal
  Monitoring, ACS Appl. Mater. Interfaces. 15 (2023) 28664-28674.
- [85] Z.-Y. Wang, X.-K. Liu, Polymer-to-Monomers Chemically Recyclable Poly(imide-imine)
  Plastics with Extreme-Condition Resistance and Flame Retardancy, Chin. J. Polym. Sci.
  42 (2024) 1525-1535.
- 43 [86] J. Zheng, H. Feng, X. Zhang, J. Zheng, J.K.W. Ng, S. Wang, N. Hadjichristidis, Z. Li, 44 Advancing Recyclable Thermosets through C=C/C=N Dynamic Covalent Metathesis 45 Chemistry, J. Am. Chem. Soc. 146 (2024) 21612-21622.
- [87] S. Pal, J. Shin, K. DeFrates, M. Arslan, K. Dale, H. Chen, D. Ramirez, P.B. Messersmith,
  Recyclable surgical, consumer, and industrial adhesives of poly(α-lipoic acid), Science.
  385 (2024) 877-883.